

Structural basis of the American mink ACE2 binding by Y453F trimeric spike glycoproteins of SARS-CoV-2

Bo Liang¹, Hyunjun Ahn¹, Brenda M. Calderon², Xiaoyu Fan², Yunrong Gao¹, Natalie L. Horgan¹, Nannan Jiang², Dylan S. Blohm¹, Jaber Hossain², Nicole Wedad K. Rayyan¹, Sarah H. Osman², Xudong Lin², Michael Currier², John Steel³, David E. Wentworth², and Bin Zhou²

¹Emory University Department of Biochemistry

²Centers for Disease Control and Prevention

³National Center for Immunization and Respiratory Diseases

July 31, 2023

Abstract

Severe Acute Respiratory Syndrome Coronavirus 2 (SARS-CoV-2) enters the host cell by binding to angiotensin-converting enzyme 2 (ACE2). While evolutionarily conserved, ACE2 glycoproteins differ across various species and differential interactions with Spike (S) glycoproteins of SARS-CoV-2 viruses impact species specificity. Reverse zoonoses led to SARS-CoV-2 outbreaks on multiple American mink (*Mustela vison*) farms during the pandemic and gave rise to mink-associated S substitutions known for transmissibility between mink and zoonotic transmission to humans. In this study, we used bio-layer interferometry (BLI) to discern the differences in binding affinity between multiple human and mink-derived S glycoproteins of SARS-CoV-2 and their respective ACE2 glycoproteins. Further, we conducted a structural analysis of a mink variant S glycoprotein and American mink ACE2 (mvACE2) using cryo-electron microscopy (cryo-EM), revealing four distinct conformations. We discovered a novel intermediary conformation where the mvACE2 glycoprotein is bound to the receptor-binding domain (RBD) of the S glycoprotein in a “down” position, approximately 34° lower than previously reported “up” RBD. Finally, we compared residue interactions in the S-ACE2 complex interface of S glycoprotein conformations with varying RBD orientations. These findings provide valuable insights into the molecular mechanisms of SARS-CoV-2 entry.

Structural basis of the American mink ACE2 binding by Y453F trimeric spike glycoproteins of SARS-CoV-2

Hyunjun Ahn¹#, Brenda M. Calderon^{2,3}#, Xiaoyu Fan^{2,3}#, Yunrong Gao¹#, Natalie L. Horgan¹, Nannan Jiang^{2,3}, Dylan S. Blohm¹, Jaber Hossain^{2,3}, Nicole Wedad K. Rayyan¹, Sarah H. Osman^{2,4}, Xudong Lin^{2,3}, Michael Currier^{2,3}, John Steel³, David E. Wentworth^{2,3}, Bin Zhou^{2,3*}, Bo Liang^{1*}

¹Department of Biochemistry, Emory University School of Medicine, Atlanta, GA, 30322 United States

²COVID-19 Emergency Response, Centers for Disease Control and Prevention, Atlanta, GA 30329

³Influenza Division, National Center for Immunization and Respiratory Diseases, Centers for Disease Control and Prevention, Atlanta, GA 30329

⁴Division of Laboratory Sciences, National Center for Environmental Health, Centers for Disease Control and Prevention, Chamblee, GA, 30341

These authors contributed equally to this study.

* Correspondence: bo.liang@emory.edu and bzhou@cdc.gov

Abstract :

Severe Acute Respiratory Syndrome Coronavirus 2 (SARS-CoV-2) enters the host cell by binding to angiotensin-converting enzyme 2 (ACE2). While evolutionarily conserved, ACE2 glycoproteins differ across various species and differential interactions with Spike (S) glycoproteins of SARS-CoV-2 viruses impact species specificity. Reverse zoonoses led to SARS-CoV-2 outbreaks on multiple American mink (*Mustela vison*) farms during the pandemic and gave rise to mink-associated S substitutions known for transmissibility between mink and zoonotic transmission to humans. In this study, we used bio-layer interferometry (BLI) to discern the differences in binding affinity between multiple human and mink-derived S glycoproteins of SARS-CoV-2 and their respective ACE2 glycoproteins. Further, we conducted a structural analysis of a mink variant S glycoprotein and American mink ACE2 (mvACE2) using cryo-electron microscopy (cryo-EM), revealing four distinct conformations. We discovered a novel intermediary conformation where the mvACE2 glycoprotein is bound to the receptor-binding domain (RBD) of the S glycoprotein in a “down” position, approximately 34° lower than previously reported “up” RBD. Finally, we compared residue interactions in the S-ACE2 complex interface of S glycoprotein conformations with varying RBD orientations. These findings provide valuable insights into the molecular mechanisms of SARS-CoV-2 entry.

1. Introduction:

Severe acute respiratory syndrome coronavirus 2 (SARS-CoV-2) causes the respiratory illness coronavirus disease 19 (COVID-19), which escalated to a global pandemic in 2020¹. SARS-CoV-2 is a positive-sense single-stranded RNA virus made up of four structural proteins, which include nucleocapsid (N), envelope (E), membrane (M), and spike (S) glycoproteins². S glycoprotein, decorated on the surface of the virus, mediates the virus entry process by binding to different host cell receptors, which includes the human angiotensin-converting enzyme 2 (hACE2), making it an important target for developing vaccines and therapeutics^{3,4}.

S glycoprotein on the mature virion is a homotrimer, with each monomer comprising two subunits: the S1 subunit containing the N-terminal domain (NTD) and the receptor-binding domain (RBD) that binds to the hACE2 receptor, and the S2 subunit containing the fusion peptide that mediates the membrane fusion of the virus and host cells^{3,5}. Rapid advances in the structural biology of the SARS-CoV-2 S glycoprotein have occurred since its initial outbreak, including pre- and post-fusion S glycoprotein, RBD-ACE2 complex, and trimeric spike-ACE2 complex⁵⁻¹⁴.

While *Rhinolophus affinis* represent the natural reservoir of precursors to SARS-CoV-2¹⁵, multiple species, in addition to humans, are susceptible to infection¹⁶⁻²⁸. In April 2020, outbreaks of SARS-CoV-2 on American mink (*Mustela vison*) farms were first reported in the Netherlands, with later outbreaks observed in mink farms throughout Europe and North America^{25,26,29,30}. The virus was transmitted to mink by infected human workers and was capable of transmission among American mink and back to humans³¹. In Denmark, sequence analysis of human samples identified five related clusters with different mutations in the S glycoprotein, and one of these, cluster 5, raised alarms internationally for harboring five mutations ([?]69-70, Y453F, D614G, I692V, M1229I) in the S glycoprotein^{31,32}. A notable mutation present in this and other clusters is Y453F, located in the RBD of the S glycoprotein, which arose via parallel evolution in independent mink outbreaks and has been shown to increase the binding and entry efficiency into cells expressing American mink ACE2 (mvACE2) while retaining its affinity to hACE2^{8,32}.

Previous studies reported the crystal and cryo-EM structures of mink variant spike RBDs in complexes with mink ACE2, providing key insights into how the Y453F mutation affects the binding of the S glycoprotein to ACE2^{8,9}. However, the structure of Y453F trimeric S glycoprotein in complex with mvACE2 has yet to be solved, and many conformational stages remain to be elucidated. In this study, we presented the cryo-EM structures of the trimeric S glycoprotein containing the cluster 5 S1 mutations (Δ 69-70, Y453F, D614G) complexed with mvACE2 receptors in various conformational stages. Notably, our study captured

an intermediate step in which mvACE2 is bound to the RBD of the S glycoprotein at a lower angle than previously reported^{13,14,33}, facilitating the further opening of the RBD. Collectively, our results provide further structural insights into the initial residue interactions between the S glycoprotein and mvACE2, and the molecular mechanisms involved in the conformational changes of the S glycoprotein upon binding to the host mvACE2 receptor.

2. Materials and Methods:

2.1. Expression and purification of the S glycoprotein and ACE2

SARS-CoV-2 S glycoprotein expression plasmids were constructed to encode the ectodomain of S glycoprotein (residues 1–1208, with a mutated furin cleavage site and two stabilizing proline substitutions K986P/V987P) followed by a T4 foldon trimerization domain and a polyhistidine purification tag, as described previously³⁴. For functional assays, different constructs were designed to encode S with mutations found in wild-type human viruses or viruses from American mink and are referred to throughout the text as S^{D614G}, S^{D614G+Y453F}, and S^{Δ614Γ+Δ69-70+Ψ453Φ}. For structural analysis, a SARS-CoV-2 S glycoprotein expression plasmid with four additional stabilizing proline mutations (F817P, A892P, A899P, A942P)³⁵ was constructed and is referred to throughout the text as mink S glycoprotein for simplicity.

ACE2 expression plasmids were also constructed as described previously to encode the ectodomain of dimeric ACE2 followed by a human IgG1 Fc purification tag, referred to throughout the text as hACE2-Fc and mvACE2-Fc³⁴. Additionally, a monomeric mink ACE2 construct, where the IgG1 Fc purification tag was replaced with a polyhistidine purification tag, was constructed for structure determination and is referred to throughout the text as mvACE2. The American mink ACE2 sequence was determined previously³⁶.

Expi293F cells (Thermo Fisher, A14527) were cultured in Expi293 Expression Medium at 37°C and 8% CO₂ in the Orbi-Shaker (Sigma, Z763438) at 130 rpm. The cells were transiently transfected at a 3.0 x 10⁶ cells/mL density using an Expifectamine 293 transfection kit (Thermofisher, A14524). For polyhistidine-tagged proteins, the supernatant was harvested by centrifugation after 72 hours and supplemented with 20 mM Imidazole, followed by affinity chromatography with Ni²⁺-NTA agarose beads (GoldBio, H-350). The sample was washed three times with 5 column volumes (CV) of wash buffer (30 mM Na₂HPO₄ pH 7.4, 500 mM NaCl, 30 mM Imidazole) and then eluted three times with 5 CVs of elution buffer (20 mM Na₂HPO₄ pH 7.4, 500 mM NaCl, 500 mM Imidazole). For Fc-tagged proteins, the supernatant was harvested by centrifugation after 72 hours, followed by affinity chromatography using HiTrap protein A columns (Cytiva). The sample was washed with 10 CVs of wash buffer (20 mM sodium phosphate, pH 7.4) and eluted with 5 CVs of elution buffer (0.1 M citric acid, pH 3). Sample collection tubes were pre-loaded with neutralization buffer (1M Tris HCl, pH 9).

The eluted proteins were concentrated with 50-kDa or 100-kDa MWCO centrifugal filters. Protein samples used for bio-layer interferometry (BLI) assays were used after affinity chromatography. Protein samples used for structure determination were further purified by size exclusion chromatography using the Superose 6 increase 10/300 GL column (Cytiva) in buffer (20 mM Tris pH 8.0, 200 mM NaCl). The peak fractions were collected and verified through SDS-PAGE gel analysis. The samples were concentrated and flash-frozen in liquid nitrogen and stored at -80°C.

2.2. Bio-layer interferometry assay

The binding affinity between the various trimeric S glycoproteins and dimeric ACE2 receptors was evaluated using the Octet RED96 instrument at 30°C with a shaking speed of 1000 RPM (ForteBio), as described previously³⁷. Anti-human IgG Fc biosensors (ForteBio) were used. Following 10 minutes of pre-hydration of anti-human IgG Fc biosensors and 1 minute of sensor check, 7.5 nM of hACE2-Fc or 15 nM of mvACE2-Fc in 10X kinetic buffer (ForteBio) were loaded onto the surface of anti-human IgG Fc biosensors for 5 minutes. After 1.5 minutes of baseline equilibration, 5 minutes of association was conducted at 10 – 100 nM S glycoprotein, followed by 5 minutes of dissociation in the same buffer used for baseline equilibration. For binding assays using mvACE2-Fc, the association was conducted with 25 – 200 nM S glycoprotein. The data

were corrected by subtracting the signal from the reference sample, and a 1:1 binding model with the global fit was used to determine equilibrium dissociation constants (Kd). Statistical analysis was performed using GraphPad Prism 9 software. Two-way analysis of variance (ANOVA) with Dunnett’s multiple comparisons test was used to compare the binding affinity (Kd) of S glycoprotein variants with hACE2-Fc or mvACE2-Fc glycoproteins, and significance was defined as $P < 0.05$.

2.3. Electron microscopy specimen preparation and data acquisition

To prepare cryo-EM samples, 3 μL of ~ 1.5 mg/mL mink S glycoprotein-mvACE2 complex (1:2.2 molar ratio S to mvACE2) were applied to glow-discharged holey carbon grids (Quantifoil Cu R1.2/1.3). The grids were blotted for 3 seconds at 100% relative humidity and flash-frozen in liquid ethane using a Vitrobot Mark IV system (Thermo Fisher Scientific). The cryo grids were imaged using a Krios cryogenic transmission electron microscope operated at 300 kV. The microscope was equipped with a Gatan K3 camera with a slit width of 20 eV, and a total of 11,392 micrographs were collected at 81,000X magnification. The image was exposed for 4.0 seconds fractionated with 40 frames with an accumulated dose of $49.98 \text{ e}^-/\text{\AA}^2$. The pixel size was 1.11 \AA with a defocus range of -0.75 to -1.75 μm .

2.4. Cryo-EM data processing

All data processing was conducted in CryoSPARC v4.1.1³⁸. Patch motion correction and CTF estimation were performed before manually curating exposures to exclude 1,746 micrographs with statistical outliers. 4,458,674 particles were initially extracted via blob particle picking from the remaining 9,646 micrographs, followed by template particle picking. Extracted particles underwent a series of 2D classifications and 3D classifications for refinement. Local refinement was further performed with a mask covering the American mink S glycoprotein RBD interacting with mvACE2. The full workflow is summarized in Figure S1.

2.5 Model building and visualization

Initial model building of the different conformations of mink S glycoprotein and the mvACE2 complex was performed in UCSF ChimeraX using PDB 6ACJ and 7LWI for global mink S-mvACE2 complex and PDB 7F5R for mink S glycoprotein RBD-mvACE2 complex after local refinement as a starting model. Several rounds of refinement in Phenix and manual building in Coot were performed until the final reliable models were obtained. Model and map statistics are summarized in Supplementary Tables 1-2.

Figures were generated using UCSF ChimeraX and PyMol. UCSF ChimeraX was used to measure the angles between the RBD and spike protein³³. The "Define" function was used to generate the horizontal plane of the American mink S glycoprotein and long axis across the RBD. The "angle" function was used to calculate the angles between the plane and the axis.

Cryo-EM reconstructions and atomic models generated in this study are available at the Protein Data Base (PDB) under the following accession codes: mink S glycoprotein alone (8T21), mink S glycoprotein bound to one mvACE2 with downRBD (8T22) or upRBD (8TAZ), mink S glycoprotein bound to two mvACE2 (8T20), and local refinement of the RBD-ACE2 interface of downRBD (8T25) and upRBD (8T23).

3. Results:

3.1. The binding of S glycoprotein homotrimers to hACE2-Fc and mvACE2-Fc

To identify potential differences in the binding affinity of S glycoproteins to hACE2-Fc or mvACE2-Fc glycoproteins, we performed bio-layer interferometry (BLI) assays. We determined the equilibrium dissociation constants (Kd) for trimeric S stabilized by 2 proline substitutions (K986P and V987P)³⁵ and harboring either the human (S^{D614G}) or American mink-associated mutations ($\text{S}^{\text{D614G+Y453F}}$ or $\text{S}^{\Delta 614\Gamma+\Delta 69-70+\Psi 453\Phi}$) from immobilized dimeric hACE2-Fc or mvACE2-Fc receptors. The S^{D614G} was chosen as it represents the pre-dominant SARS-CoV-2 viruses circulating in humans when the variants infecting American mink emerged. The trimeric S glycoproteins S^{D614G} , $\text{S}^{\text{D614G+Y453F}}$, and $\text{S}^{\Delta 614\Gamma+\Delta 69-70+\Psi 453\Phi}$ all bound to dimeric hACE2-Fc receptor with similar affinity, and no statistically significant differences were observed (Fig. 1). However, the S^{D614G} displayed a 5-fold reduction in affinity when the hACE2-Fc was substituted with mvACE2-Fc

in the assay. The affinity of S for mvACE2-Fc was restored to S^{D614G}-hACE2-Fc levels by the Y453F mutation in the spike, as both S^{D614G+Y453F} and S^{Δ614Γ+Δ69-70+Ψ453Φ} showed a >4-fold increase of affinity to mvACE2-Fc, compared to S^{D614G} ($p < 0.0001$). The Δ69-70 deletion in NTD didn't further increase the binding affinity to mvACE2-Fc beyond the effect of the Y453F RBD mutation (Fig. 1).

3.2. Cryo-EM structural determination

To facilitate structure determination, we prepared a trimeric mink S glycoprotein, harboring some of the mutations (Δ69-70, Y453F, D614G) found in mink cluster 5, with six proline substitutions that are reported to have increased protein yields and stability in the prefusion state³⁵. We mixed the mink S glycoprotein with monomeric mvACE2 at a molar ratio of 1:2.2 and incubated it for 15 minutes before subjecting the complex to vitrification for EM analysis.

Cryo-EM analysis of the complex determined four distinctive species: mink S glycoprotein alone (13.8%), mink S glycoprotein bound to one mvACE2 with downRBD (16.0%) or upRBD (14.3%), and mink S glycoprotein bound to two mvACE2 in the upRBD position (55.8%) (Fig. 2). After 3D classification and refinement, apo-mink S glycoprotein was resolved at 3.60 Å, while three conformational states of the mink S glycoprotein-mvACE2 complex were captured and determined at 3.83 Å, 3.75 Å, and 3.36 Å. The RBDs were flexible with respect to the horizontal plane of the spike protein, as shown by the 2D and 3D classification analysis, capturing four different RBD angles: 27.1°, 28.9°, 62.8°, and 69.2° (Fig. S1F and 2).

Cryo-EM structural analysis of the mink S glycoprotein shows that its overall organization of the trimer is similar to other variants, including Alpha, Delta, Omicron, and previously published mink S glycoprotein (Fig. 3). Our captured apo-mink S glycoprotein was determined to have three receptor binding domains in the down position. The RBDs of the mink S glycoprotein structures are less well-resolved, most likely due to its flexibility in the region compared to the rest of the protein chain. However, it is clear that the overall architecture of the different S variants is conserved, which is consistent with the conserved high affinity for hACE2 receptor.

3.3 Structure of SARS-CoV-2 S glycoprotein trimer with downRBD bound to mvACE2

In our cryo-EM analysis, we found that 30.3% of the species were composed of the S glycoprotein bound to a single mvACE2 receptor (Fig. 2B and 2C). 16% of the single mvACE2 bound species had strong density for mvACE2 bound to an RBD at an angle of 28.9° ("downRBD") (Fig. 2B), while the other 14.3% (Fig. 2C) had strong density at an angle of 62.8° ("upRBD"). The mvACE2 bound to the downRBD-spike (Fig. 2B) represents a novel intermediary conformation that has not been previously captured. Previous studies have suggested that the spike protein can only accommodate ACE2 binding when its RBD is up at an angle of at least 50° with respect to the horizontal plane of the spike protein^{14,33,39}.

To further elucidate the mechanism of this conformation, we resolved the complex structure of mvACE2 bound to downRBD-spike at 3.75 Å (Fig. 4A, S1C, and S1E). The structure was further improved using local refinement covering the mink S glycoprotein RBD-mvACE2 interface, returning a 3.62 Å resolution of the density map (Fig. 4B, S1H, and S1J). To analyze the binding interface between the complex, we selected residues located less than 4.0 Å apart⁴⁰ (Fig 4C). Structural analysis (Fig. 4C-F) revealed that the binding of the two molecules in the conformation is mediated by π -cation interaction between S R403 and mvACE2 Y34 and between S Y505 and mvACE2 R393, π - π stacking between S F486 and mvACE2 H79 and between S Y505 and mvACE2 H354, and ionic interaction between S K417 and mvACE2 E30. Multiple sequence alignments of different S glycoprotein variants show that these participating residues are mostly well conserved (Fig. 3). Interestingly, we found that S F453 does not form hydrophobic, π - π stacking or any contact interaction with the mvACE2 Y34 (Fig. 4C and 4F), contrary to when the mvACE2 is bound to upRBD of the spike, as it was previously reported^{8,9} and as will be demonstrated in the following section.

3.4 Structure of SARS-CoV-2 S glycoprotein trimer with upRBD bound to mvACE2 receptor

One of the three mvACE2-bound spike trimers captured had a strong density for mvACE2 bound to two of the RBD at 69.2°. After multiple rounds of additional 2D and 3D classification analysis, we determined

the complex structure of mink S glycoprotein bound to two mvACE2 at 3.36 Å (Fig. 5A, S1B, and S1D). The local resolution of the protein interface between the complex was low due to its flexibility in the region. Nonetheless, the overall architecture of the mvACE2-mink S glycoprotein complex was comparable to the previously published structure. To visualize the key interaction at the protein interface between the complex, we performed local refinement with the mask covering the RBD-ACE2 interface, returning the improved resolution of the density map at 3.82Å (Fig. 5B, S1G, and S1I). To analyze the binding interface between the complex, we selected residues located less than 4.0 Å apart⁴⁰ (Fig 5C).

Overall, our structure largely agreed with the previous Y453F RBD-mink ACE2 in interface residues^{8,9} (Fig. 5D-F). Notable interactions include a salt bridge between mink S D405 with mvACE2 H354 and S E484 with mvACE2 H79; hydrogen bond between S T500 with mvACE2 Y41, S G502 with mvACE2 K353, and S Y505 with mvACE2 R393; π -cation interaction between S Y489 with mvACE2 K31; and π - π stacking between S F453 with mvACE2 Y34 and S Y505 with mvACE2 H354. F453 in S glycoprotein is unique to the mink variant among other S variants (Fig. 3), and as indicated in our structural and binding affinity studies, as well as noted in previous studies^{8,9}, Y453F mink S glycoprotein enhances the interaction with mvACE2 Y34.

3.5. The conformational changes of mink S glycoprotein with mvACE2 receptor

Herein, we performed a simultaneous structural comparison of mvACE2-unbound and mvACE2-bound to spike at various RBD angles to investigate the different conformational changes induced by binding. Previous studies have reported that spike glycoprotein could only accommodate ACE2 binding when its RBD is up at an angle of at least 50° with respect to the horizontal plane of the S glycoprotein^{14,33,39}. However, this data shows that about half of the mink S glycoprotein bound to one mvACE2 accommodated the mvACE2 binding with the RBD at a lower angle than previously reported^{13,14,33} (Fig. 2 and 6A).

Further structural comparison of our density map shows that the mvACE2-free conformation had its RBD at 27.1° in relation to the horizontal plane of mink S glycoprotein (Fig 2A). In comparison, one mvACE2 and two mvACE2 bound spikes had their RBD rotate outward with an up position at 62.8° and 69.2°, respectively (Fig 2C and 2D). The angle at which mvACE2 is bound to the upRBD in our study is comparable to the angles previously reported^{14,33,39} (Fig 6B and 6C). The intermediate stage of the mvACE2-bound mink S glycoprotein with downRBD captured was at an angle of 28.9°, similar to the angle of mvACE2-free conformation and approximately 34°- 40° lower than when it had up RBD (Fig. 6A). These findings challenge the previously reported notion that ACE2 binding may only occur when the RBD is up at a high angle as well as provide insight into the conformational changes that are induced upon ACE2 binding.

4. Discussion:

Our *in vitro* binding studies demonstrate a weaker binding affinity of the S^{D614G} protein to the mvACE2 receptor compared to the hACE2 receptor, and this suboptimal fitness in a new host may be overcome by selecting virus with host-adaptive mutations. Indeed, mutations were frequently observed in SARS-CoV-2 isolates derived from infected mink^{26,41}. We show that the addition of the mink-associated S glycoprotein mutations $\Delta 69-70$ and Y453F enhance binding to mvACE2 while having little impact on binding to the hACE2 receptor, suggesting they are host-adaptive mutations to American mink. The similarity in binding affinity between S^{D614G+Y453F} and S ^{$\Delta 614G+\Delta 69-70+\Psi 453\Phi$} with the mvACE2 receptor suggests that the Y453F change is the main driver of the observed enhanced binding to mvACE2. Y453F has been shown by others to enhance mustelid ACE2 usage^{8,9,42}. Residue 453 is located in the S glycoprotein RBD and interacts with hACE2 receptor residue H34, which is a Y34 in mvACE2. To elucidate the enhanced mvACE2 receptor binding mechanism, we solved the structure of the American mink S glycoprotein trimer bound to the mvACE2 receptor.

As previously reported, the RBD was at a range of tilts and angles regarding the horizontal plane of spike³³. The general consensus was that the RBD of the spike protein undergoes a conformational shift in its RBD from an inactive "down" state to an active "up" state at an angle of at least 50° to access the ACE2 of the host cell^{14,33,39}. Our study captured a novel intermediate step in which the mvACE2 binds to mink S glycoprotein with the RBD at a relatively lower angle than previously reported (Fig 4 and 6A). The

simultaneous structural comparison suggests that the binding of the mvACE2 receptor facilitates the further opening of the CTD1 of the S glycoprotein. This would expose the fusion cleavage site of S2 in the spike, triggering the release of the S1 subunit from the S glycoprotein trimer⁴³.

Overall, our structural analysis of the full trimeric mink S-mvACE2 complex is mainly in agreement with previously published structures⁵⁻¹⁴ in its architecture. Additionally, comparing the molecular interface between previously published mink S RBD-mink ACE2 complex and our full trimeric mink S-mvACE2 complex when RBD is up at $>50^\circ$ revealed comparable interacting residues^{8,9} (Fig 6). This includes the enhanced interaction between S F453 with mvACE2 Y34 via π - π stacking from the Y453F substitution mutation in the mink S glycoprotein.

Further analysis of the mink S-mvACE2 complex revealed that the interacting residues in the interface of the mink S and mvACE2 molecules differ depending on the angle at which the RBD is bound to mvACE2 (Fig 5C and 6C). These results provide insights into the residues in the spike trimer that are important for initiating the binding of the host ACE2 receptor. For example, while we observed that S R403, K417, and F486 may play a role in initiating the binding of the ACE2 receptor, we did not note any interaction in these residues when the ACE2 is bound to S at a higher angle. Similarly, we note that S Y505 plays a role in both initiating and maintaining the binding of host ACE2 receptors. This is congruent with previous reports that Y505 is a critical viral determinant for specific recognition of ACE2 by SARS-CoV-2 RBD and why many potent neutralizing antibodies interact with this specific residue^{42,44,45}. Overall, our sequence alignment indicates that these interacting residues of the spike in downRBD conformation are well-conserved across different variants except the Y505H substitution in the Omicron BA.1 variant (Fig 3). It is reported that while the Y505H mutation in Omicron BA.1 significantly reduced ACE2 binding, and other mutations in the RBD compensated for its decreased binding affinity^{13,46}.

The interactions between SARS-CoV-2 S glycoproteins and ACE2 receptors are of prime interest due to the essential role it plays in species specificity, transmission and pathogenesis. SARS-CoV-2 is now endemic in humans and will give rise to periodic epidemics similar to that of influenza A and B viruses and respiratory syncytial virus. Mutations will continue to emerge in the S glycoprotein to escape host immunity and/or optimize interactions with hACE2, and performing similar structural studies on new variants is necessary for understanding the disease and updating vaccines. Monitoring S glycoprotein variants for expanded or altered species specificity will also help assess the risk of zoonosis and reverse zoonosis.

ACKNOWLEDGMENTS

We thank the assistance and services provided at the Robert P. Apkarian Integrated Electron Microscopy Core (IEMC) at Emory University. This research was partly supported by the National Cancer Institute's National Cryo-EM Facility at the Frederick National Laboratory for Cancer Research under contract 75N91019D00024. This project was supported in part by an appointment to the Research Participation Program at the Centers for Disease Control and Prevention, administered by the Oak Ridge Institute for Science and Education through an interagency agreement between the U.S. Department of Energy and CDC. The findings and conclusions in this report are those of the authors and do not necessarily represent the official position of the U.S. Centers for Disease Control and Prevention or the Agency for Toxic Substances and Disease Registry.

CONFLICTS OF INTEREST

The authors declare that there are no conflicts of interest.

REFERENCES

1. Wu D, Wu T, Liu Q, Yang Z. The SARS-CoV-2 outbreak: What we know. *Int J Infect Dis.* 2020;94:44-48.
2. Kim D, Lee JY, Yang JS, Kim JW, Kim VN, Chang H. The Architecture of SARS-CoV-2 Transcriptome. *Cell.* 2020;181(4):914-921 e910.

3. Ke Z, Oton J, Qu K, et al. Structures and distributions of SARS-CoV-2 spike proteins on intact virions. *Nature*. 2020;588(7838):498-502.
4. Shirbhate E, Pandey J, Patel VK, et al. Understanding the role of ACE-2 receptor in pathogenesis of COVID-19 disease: a potential approach for therapeutic intervention. *Pharmacol Rep*.2021;73(6):1539-1550.
5. Cai Y, Zhang J, Xiao T, et al. Distinct conformational states of SARS-CoV-2 spike protein. *Science*. 2020;369(6511):1586-1592.
6. Wrapp D, Wang N, Corbett KS, et al. Cryo-EM structure of the 2019-nCoV spike in the prefusion conformation. *Science*.2020;367(6483):1260-1263.
7. Zhang J, Cai Y, Xiao T, et al. Structural impact on SARS-CoV-2 spike protein by D614G substitution. *Science*. 2021;372(6541):525-530.
8. Ren W, Lan J, Ju X, et al. Mutation Y453F in the spike protein of SARS-CoV-2 enhances interaction with the mink ACE2 receptor for host adaptation. *PLoS Pathog*. 2021;17(11):e1010053.
9. Su C, He J, Han P, et al. Molecular Basis of Mink ACE2 Binding to SARS-CoV-2 and Its Mink-Derived Variants. *J Virol*.2022;96(17):e0081422.
10. Lan J, Ge J, Yu J, et al. Structure of the SARS-CoV-2 spike receptor-binding domain bound to the ACE2 receptor. *Nature*.2020;581(7807):215-220.
11. Shang J, Ye G, Shi K, et al. Structural basis of receptor recognition by SARS-CoV-2. *Nature*. 2020;581(7807):221-224.
12. Wang Q, Zhang Y, Wu L, et al. Structural and Functional Basis of SARS-CoV-2 Entry by Using Human ACE2. *Cell*. 2020;181(4):894-904 e899.
13. Mannar D, Saville JW, Zhu X, et al. SARS-CoV-2 Omicron variant: Antibody evasion and cryo-EM structure of spike protein-ACE2 complex. *Science*. 2022;375(6582):760-764.
14. Benton DJ, Wrobel AG, Xu P, et al. Receptor binding and priming of the spike protein of SARS-CoV-2 for membrane fusion. *Nature*.2020;588(7837):327-330.
15. Zhou P, Yang XL, Wang XG, et al. A pneumonia outbreak associated with a new coronavirus of probable bat origin. *Nature*.2020;579(7798):270-273.
16. Ji W, Wang W, Zhao X, Zai J, Li X. Cross-species transmission of the newly identified coronavirus 2019-nCoV. *J Med Virol*.2020;92(4):433-440.
17. McAloose D, Laverack M, Wang L, et al. From People to Panthera: Natural SARS-CoV-2 Infection in Tigers and Lions at the Bronx Zoo. *mBio*. 2020;11(5).
18. Patterson EI, Elia G, Grassi A, et al. Evidence of exposure to SARS-CoV-2 in cats and dogs from households in Italy. *Nat Commun*.2020;11(1):6231.
19. Ruiz-Arrondo I, Portillo A, Palomar AM, et al. Detection of SARS-CoV-2 in pets living with COVID-19 owners diagnosed during the COVID-19 lockdown in Spain: A case of an asymptomatic cat with SARS-CoV-2 in Europe. *Transbound Emerg Dis*. 2021;68(2):973-976.
20. Shi J, Wen Z, Zhong G, et al. Susceptibility of ferrets, cats, dogs, and other domesticated animals to SARS-coronavirus 2. *Science*.2020;368(6494):1016-1020.
21. Sit THC, Brackman CJ, Ip SM, et al. Infection of dogs with SARS-CoV-2. *Nature*. 2020;586(7831):776-778.
22. Munster VJ, Feldmann F, Williamson BN, et al. Respiratory disease in rhesus macaques inoculated with SARS-CoV-2. *Nature*.2020;585(7824):268-272.

23. Woolsey C, Borisevich V, Prasad AN, et al. Establishment of an African green monkey model for COVID-19 and protection against re-infection. *Nat Immunol.* 2021;22(1):86-98.
24. Lam TT, Jia N, Zhang YW, et al. Identifying SARS-CoV-2-related coronaviruses in Malayan pangolins. *Nature.*2020;583(7815):282-285.
25. Badiola JJ, Otero A, Sevilla E, et al. SARS-CoV-2 Outbreak on a Spanish Mink Farm: Epidemiological, Molecular, and Pathological Studies. *Front Vet Sci.* 2021;8:805004.
26. Hammer AS, Quaade ML, Rasmussen TB, et al. SARS-CoV-2 Transmission between Mink (*Neovison vison*) and Humans, Denmark. *Emerg Infect Dis.* 2021;27(2):547-551.
27. Koopmans M. SARS-CoV-2 and the human-animal interface: outbreaks on mink farms. *Lancet Infect Dis.* 2021;21(1):18-19.
28. Fritz M, de Riols de Fonclare D, Garcia D, et al. First Evidence of Natural SARS-CoV-2 Infection in Domestic Rabbits. *Vet Sci.*2022;9(2).
29. Oreshkova N, Molenaar RJ, Vreman S, et al. SARS-CoV-2 infection in farmed minks, the Netherlands, April and May 2020. *Euro Surveill.*2020;25(23).
30. Domanska-Blicharz K, Orłowska A, Smreczak M, et al. Mink SARS-CoV-2 Infection in Poland - Short Communication. *J Vet Res.*2021;65(1):1-5.
31. Oude Munnink BB, Sikkema RS, Nieuwenhuijse DF, et al. Transmission of SARS-CoV-2 on mink farms between humans and mink and back to humans. *Science.* 2021;371(6525):172-177.
32. Larsen CS, Paludan SR. Corona's new coat: SARS-CoV-2 in Danish minks and implications for travel medicine. *Travel Med Infect Dis.*2020;38:101922.
33. Song W, Gui M, Wang X, Xiang Y. Cryo-EM structure of the SARS coronavirus spike glycoprotein in complex with its host cell receptor ACE2. *PLoS Pathog.* 2018;14(8):e1007236.
34. Zhou B, Thao TTN, Hoffmann D, et al. SARS-CoV-2 spike D614G change enhances replication and transmission. *Nature.*2021;592(7852):122-127.
35. Hsieh CL, Goldsmith JA, Schaub JM, et al. Structure-based design of prefusion-stabilized SARS-CoV-2 spikes. *Science.*2020;369(6510):1501-1505.
36. Heller LK, Gillim-Ross L, Olivieri ER, Wentworth DE. *Mustela vison* ACE2 functions as a receptor for SARS-coronavirus. *Adv Exp Med Biol.* 2006;581:507-510.
37. Ulrich L, Halwe NJ, Taddeo A, et al. Enhanced fitness of SARS-CoV-2 variant of concern Alpha but not Beta. *Nature.*2022;602(7896):307-313.
38. Punjani A, Rubinstein JL, Fleet DJ, Brubaker MA. cryoSPARC: algorithms for rapid unsupervised cryo-EM structure determination. *Nat Methods.* 2017;14(3):290-296.
39. Gui M, Song W, Zhou H, et al. Cryo-electron microscopy structures of the SARS-CoV spike glycoprotein reveal a prerequisite conformational state for receptor binding. *Cell Res.* 2017;27(1):119-129.
40. Wang J, Youkharibache P, Zhang D, et al. iCn3D, a web-based 3D viewer for sharing 1D/2D/3D representations of biomolecular structures. *Bioinformatics.* 2020;36(1):131-135.
41. Laurini E, Marson D, Aulic S, Fermeglia A, Pricl S. Computational Mutagenesis at the SARS-CoV-2 Spike Protein/Angiotensin-Converting Enzyme 2 Binding Interface: Comparison with Experimental Evidence. *ACS Nano.* 2021;15(4):6929-6948.
42. Laurini E, Marson D, Aulic S, Fermeglia A, Pricl S. Molecular rationale for SARS-CoV-2 spike circulating mutations able to escape bamlanivimab and etesevimab monoclonal antibodies. *Sci Rep.*2021;11(1):20274.

43. Lu L, Sikkema RS, Velkers FC, et al. Adaptation, spread and transmission of SARS-CoV-2 in farmed minks and associated humans in the Netherlands. *Nat Commun.* 2021;12(1):6802.
44. Xu C, Wang Y, Liu C, et al. Conformational dynamics of SARS-CoV-2 trimeric spike glycoprotein in complex with receptor ACE2 revealed by cryo-EM. *Sci Adv.* 2021;7(1).
45. Yi C, Sun X, Lin Y, et al. Comprehensive mapping of binding hot spots of SARS-CoV-2 RBD-specific neutralizing antibodies for tracking immune escape variants. *Genome Med.* 2021;13(1):164.
46. Geng Q, Shi K, Ye G, Zhang W, Aihara H, Li F. Structural Basis for Human Receptor Recognition by SARS-CoV-2 Omicron Variant BA.1. *J Virol.* 2022;96(8):e0024922.

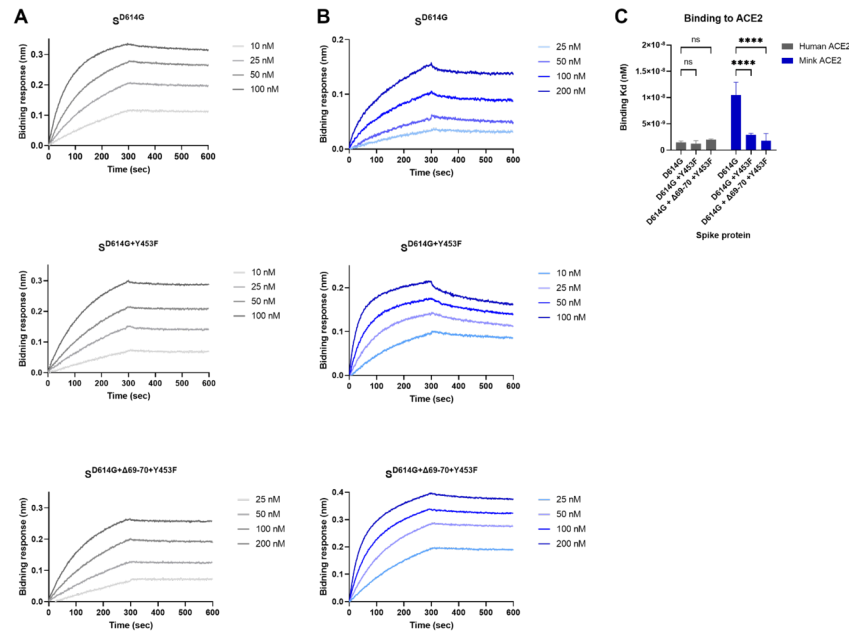


Figure 1. Binding of S glycoprotein trimers to hACE2-Fc and mvACE2-Fc receptors. (A) Representative binding profiles of S glycoprotein trimers to the hACE2-Fc receptor. The hACE2-Fc receptor was immobilized to biosensors, and binding to S glycoprotein trimers (S^{D614G}, S^{D614G+Y453F}, and S^{Δ614G+Δ69-70+Ψ453F}) was measured by bio-layer interferometry. (B) Representative binding profiles of S glycoprotein trimers to dimeric mvACE2-Fc receptors. The mvACE2-Fc receptor was immobilized to biosensors and binding to S glycoprotein trimers (S^{D614G}, S^{D614G+Y453F}, and S^{Δ614G+Δ69-70+Ψ453F}) was measured by bio-layer interferometry (C) Comparison of binding affinity (Kd) measured by bio-layer interferometry of S glycoprotein trimers to hACE2-Fc or mvACE2-Fc receptors.

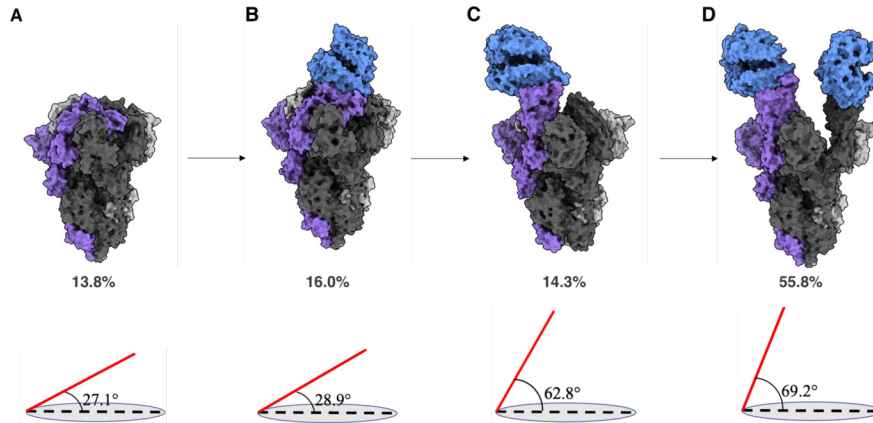


Figure 2. Electron density map of the mink ACE2-free and mvACE2 bound SARS-CoV-2 mink S glycoprotein. Diagram illustrating the density map of ACE2-free mink S glycoprotein [PDB: 8T21], one mvACE2-bound mink S glycoprotein [PDB: 8T22 and 8TAZ], and two mvACE2-bound mink S glycoproteins [PDB: 8T20]. The relative percent sample of each population is 13.8% (A), 16.0% (B), 14.3% (C), and 55.8% (D). The angle between the long axes of RBD and the horizontal plane is also shown below each species.

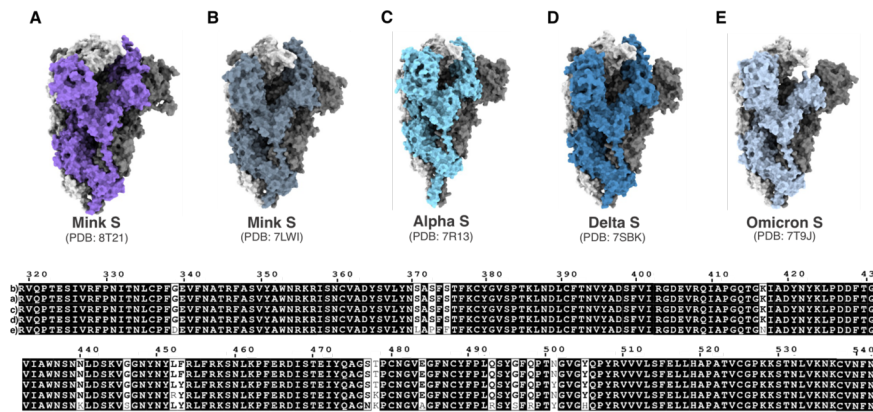


Figure 3 . Comparison of different apo spike glycoprotein variants. Structural comparison of the apo-mink S glycoprotein determined in this study [PDB: 8T21] (A) with previously reported apo-mink S glycoprotein [PDB ID: 7LWI] (B), Alpha S [PDB: 7R13] (C), Delta S [PDB: 7SBK] (D), and Omicron S [PDB: 7T9J] (E). The sequence alignment of the S glycoproteins RBD is shown below, and the conserved residues are indicated in black. Notable mutations in the mink S glycoprotein include substitution mutation Y453F.

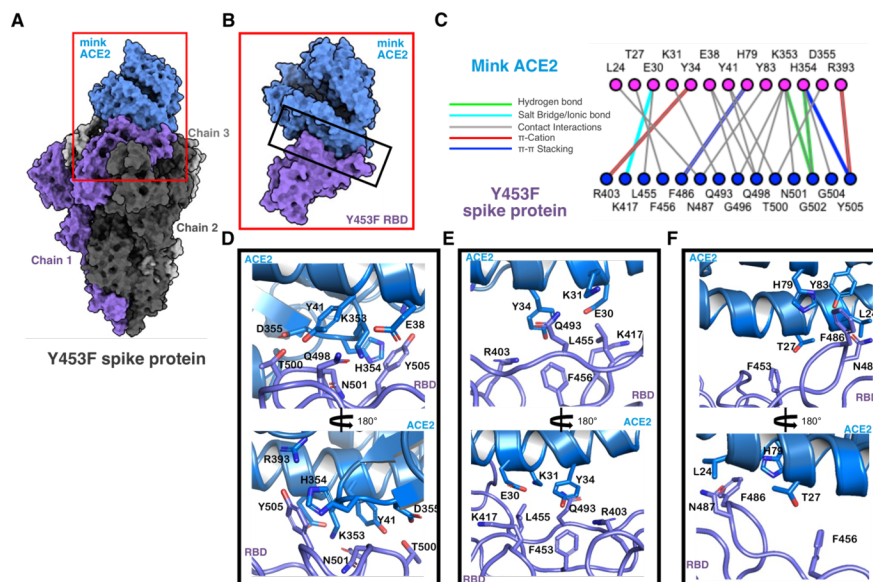


Figure 4. Cryo-EM structure of mvACE2 bound downRBD in SARS-CoV-2 mink S glycoprotein. (A) Cryo-EM map of downRBD spike glycoprotein-mvACE2 complex at 3.75 Å resolution. (B) Cryo-EM map of the Mink S glycoprotein RBD with mvACE2 after local refinement at 3.62 Å [PDB: 8T25] (C) Contacting residues less than 4 Å are labeled, and lines indicate the interactions. Hydrogen bonds, contact, pi-cation, and pi-pi stacking interactions are indicated by green, cyan, magenta, red, and blue, respectively. (D-F) Close-up view of the RBD-ACE2 interface, with key interacting residues labeled.

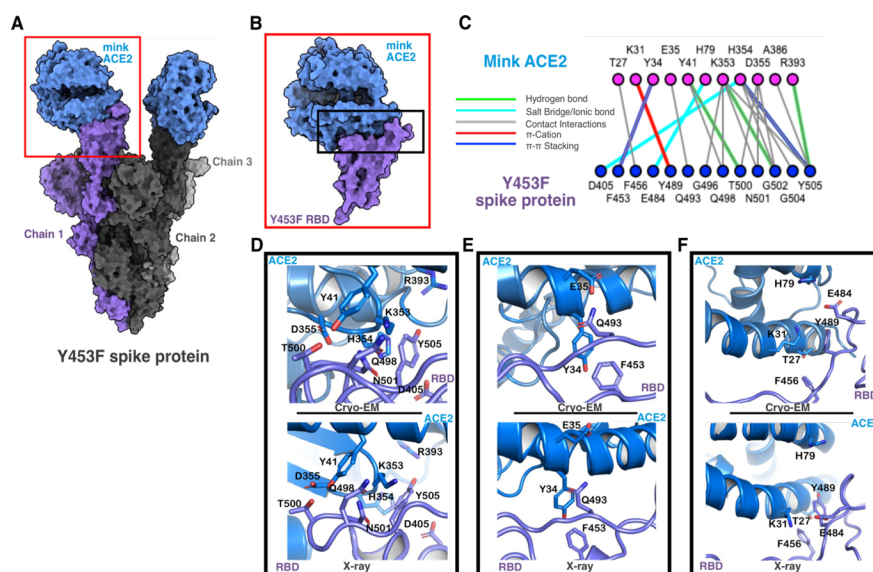


Figure 5. Cryo-EM structure of two mvACE2 bound to upRBD in SARS-CoV-2 mink S glycoprotein. (A) Cryo-EM map of upRBD mink S glycoprotein-mvACE2 complex at 3.36 Å. (B) Cryo-EM map of the Mink S glycoprotein RBD with mvACE2 after local refinement at 3.82 Å [PDB: 8T23]. (C) Contacting residues located less than 4 Å are labeled, and lines indicate the interactions. Hydrogen bonds, ionic, contact, pi-cation, and pi-pi stacking interactions are indicated by green, cyan, magenta, red, and blue, respectively. (D-F) Comparison of the close-up view of the RBD-ACE2 interface between the interface of Cryo-EM and X-ray.

the trimeric spike cryo-EM structure (top panel) and of the Y453F RBD-ACE in the x-ray crystal structure [PDB: 7F5R] (bottom panel). The key interacting residues are labeled.

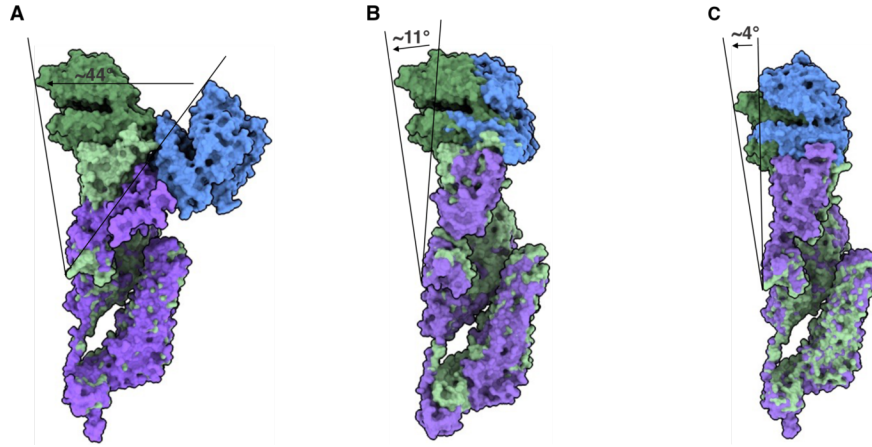


Figure 6. Superimposition of the surface density of SARS-CoV-2 mink S glycoprotein bound to mvACE2. (A) Comparison of previously reported spike chain of the trimer bound to mvACE2 complex [green; PDB ID: 6ACJ] with one mvACE2 bound S glycoprotein with downRBD [PDB ID: 8T22], (B) one mvACE2-bound S glycoprotein with upRBD [PDB ID: 8TAZ], (C) two mvACE2-bound S glycoprotein with upRBD [PDB ID: 8T20].